Gridless Joint Delay-DoA-Doppler Estimation Using OFDM Signals: A Multilevel Hankel Matrix Approach

1st Ziyu Zhou
Department of Electrical and Electronic Engineering
Imperial College London
London, UK
ziyu.zhou20@imperial.ac.uk

2nd Wei Dai
Department of Electrical and Electronic Engineering
Imperial College London
London, UK
wei.dai1@imperial.ac.uk

***Abstract*—This paper investigates the problem of joint estimation of delay, direction of arrival (DoA), and Doppler when an orthogonal frequency-division multiplexing (OFDM) signal is used for probing. A gridless approach is taken where the above three parameters live on a continuous space rather than a discrete grid. A low-rank multilevel Hankel matrix is used to capture the underlying structure of the back-scattered signals. A convex optimization, termed as Hankel nuclear norm minimization (HNNM), is developed for denoising and parameter estimation, and solved by alternating direction method of multipliers (ADMM). Simulations demonstrate that HNNM is robust to noise, and can go beyond the minimum separation bound required by another gridless method atomic norm minimization.**

***Index Terms*—gridless sparse method, Hankel matrix, nuclear norm, orthogonal frequency-division multiplexing (OFDM), super-resolution**

I. Introduction

This paper focuses on sensing via orthogonal frequency-division multiplexing (OFDM) signals. OFDM plays an important role in both wireless communications and sensing, and shows great potential for joint radar and communications systems [1], [2]. It supports high-rate data transmission for communications, simplifies signal processing for radar estimation and communication equalization, and allows the usage of the same hardware platform to perform sensing and communications. OFDM based dual-functionality systems have become research and industry hotspots in applications such as autonomous driving [3], [4].

The classical signal processing for delay and Doppler estimation is correlation-based [5]. The back-scattered signals are matched-filtered using the transmitted signal. Targets can then be detected by searching for the proper signal delay and Doppler. In this setting, the width of the main lobe of the correlation function decides resolution, which is the minimum gap between two point targets that are distinguishable.

The rise of sparse signal processing [6] helps in improving resolution when the number of targets is small. Use delay estimation as an example. Fit the delay with a fine discrete grid, of which the gap between adjacent grid points can be smaller than the resolution of matched filtering. Though the resulted linear equation system is underdetermined, sparse recovery techniques such as orthogonal matching pursuit (OMP) [7] and subspace pursuit [8] can provide reasonably accurate estimates. However, there is a limit on how fine the discrete grid can be [9]. Superfine grid not only results in huge computational complexity but also leads to strong coherence in signal dictionary and the failure of sparse recovery [10].

Recently gridless techniques have received more and more attention. They also require small number of targets but parameters of the targets can live on a continuous space rather than a discrete grid [11]. One well-established technique is multiple signal classification (MUSIC) [12]. Its core is to identify the signal and noise subspaces from back-scattered signals. The subspace identification step is achieved by straightforward singular value decomposition (SVD) without considering possible structures of the subspaces [13]. It may not perform well at low signal-to-noise ratios (SNRs).

A modern gridless technique is atomic norm minimization (ANM) [14]–[16]. ANM can be written as a convex semidefinite programming involving a low-rank Toeplitz matrix. This Toeplitz matrix enforces the structure of the signal space, which gives ANM a greater robustness to noise compared to MUSIC [17]. However, it is well known that ANM has minimum separation requirement, meaning that it may fail if the distance between two targets is smaller than the separation bound [10], [15].

Motivated by the recent advances of multidimensional harmonic retrieval [11], [18] and passive radar sensing [5], we develop a gridless approach using Hankel matrices, termed as Hankel nuclear norm minimization (HNNM). In particular, we are interested in using HNNM to jointly estimate delay, direction of arrival (DoA), and Doppler when OFDM is used as the probing signal. Similar to ANM, HNNM makes sure that the estimated signal subspaces are generated from exponential vectors, and hence is expected to be noise-robust. At the same time, it has been shown in [19] that in theory there is no minimum separation requirement for Hankel matrix approach.

Similarly, [20] also recovers the delay, DoA and Doppler

by utilizing a Hankel related approach called Hankel matrix nuclear norm regularized low-CP-rank tensor completion (HMRTC) [18]. Nonetheless, the optimization formulation given in [20] is non-convex, and the parameters are separately estimated, leading to obtaining suboptimal parameter estimations [21].

In this paper, we first show that the received signal can be modeled by a linear operator acting on an outer product of exponential vectors. We then apply HNNM to the received signal for the purpose of joint parameter estimation. HNNM starts by constructing a low-rank multilevel Hankel matrix to capture the signal structure, then attempts parameter estimation via nuclear norm minimization of this multilevel Hankel matrix. In numerical simulations, HNNM is compared with on-grid method OMP and gridless method MUSIC. Results demonstrate that HNNM is not only robust to noise but also can go beyond the minimum separation required by ANM.

II. Signal Model and Structures

Consider an OFDM signal. A baseband time-domain OFDM signal that contains M consecutive OFDM blocks can be written as [4]

$$x(t) = \sum_{m=0}^{M-1} x_m(t - mT'), \tag{1}$$

where $x_m(t)$ denotes the OFDM symbol in the m-th OFDM block, $T' = T + T_{cp}$ is the OFDM symbol duration, T is the elementary symbol duration and T_{cp} is the cyclic prefix duration. Each OFDM symbol can be written as

$$x_m(t) = \sum_{n=-N/2}^{N/2-1} s_m[n] e^{j2\pi n \Delta_f t} c(t), \tag{2}$$

where N is the number of orthogonal subcarriers, $s_m[n]$ denotes the complex modulation symbol corresponding to the n-th subcarrier, $\Delta_f = 1/T$ represents subcarrier spacing, and $c(t)$ denotes a rectangular window function with amplitude 1 for $0 \le t \le (T_{cp} + T)$ and 0 otherwise [4].

The baseband signal is up-converted to $\tilde{x}(t) = e^{j2\pi f_c t} x(t)$ where f_c is the carrier frequency, and then transmitted.

Suppose that the received signal is back-scattered from K many targets. Index the back-scattered signal components by k. Each is characterized by the associated attenuation A_k, round-trip propagation delay $\tau_k = 2R_k/c$, and Doppler shift $f_{d,k} = f_c(2v_k/c)$ [4], where R_k and v_k are the target's range and speed relative to the receiver respectively, and c is the speed of light. Further assume that the receiver is equipped with a uniform linear antenna array composed of L many antenna elements. The uniform inter-element spacing d is assumed to be a half wavelength $\lambda/2 = c/2f_c$. Denote the DoA of the back-scattered signal from k-th target by θ_k, and θ_k is the azimuth. Hence, the received signal at the l-th antenna element is then given by

$$y_l(t) = \sum_{k=1}^{K} A_k e^{j2\pi f_{d,k} t} e^{-j\pi l \cos(\theta_k)} x(t - \tau_k) + w_l(t), \tag{3}$$

where $w(t)$ represents the additive noise.

Applying the Fourier transform to the received signal in the m-th OFDM block. As derived in [5], the n-th subcarrier signal received at the l-th antenna element can be written as

$$\begin{aligned} \tilde{Y}_{l,n}^{(m)} :=& \int_0^T e^{-j2\pi n \Delta_f t} y_l(t + mT') dt \\ \approx& T s_m[n] \sum_{k=1}^{K} \Big(A_k \\ & e^{-j\pi \left[l\cos(\theta_k) - (2m+1) f_{d,k} T' + 2n\Delta_f \tau_k \right]} \Big) + W_{l,m,n}, \end{aligned} \tag{4}$$

where the approximation is based on the fact that $f_{d,k}$ is typically small and hence $e^{j2\pi f_{d,k} t} \approx e^{j2\pi f_{d,k} T'/2} = e^{j\pi f_{d,k} T'}$ for $t \in [0, T]$ [5]. $W_{l,m,n}$ is i.i.d. Gaussian distributed.

Arrange $\tilde{Y}_{l,n}^{(m)}$ into a 3-way tensor indexed by l, m and n, and denote it by $\tilde{\boldsymbol{Y}}$ with slight abuse of notations. Then (4) can be reformulated as

$$\tilde{Y}_{l,n}^{(m)} \approx T s_m[n] B_{l,m,n} + W_{l,m,n}. \tag{5}$$

Then the tensor form of (4) is

$$\tilde{\boldsymbol{Y}} \approx \mathcal{A}(\boldsymbol{B}) + \boldsymbol{W}, \tag{6}$$

where $\mathcal{A}(.)$ is a linear operator defined via (5), $\boldsymbol{B} \in \mathbb{C}^{L \times M \times N}$ is a rank K tensor given by

$$\begin{aligned} \boldsymbol{B} =& \sum_{k=1}^{K} A_k e^{j\pi f_{d,k} T'} \boldsymbol{a}^L \left(\frac{1}{2} \cos(\theta_k) \right) \\ & \circ \boldsymbol{a}^M \left(-f_{d,k} T' \right) \circ \boldsymbol{a}^N \left(\Delta_f \tau_k \right), \end{aligned} \tag{7}$$

$$\boldsymbol{a}^L(\alpha) = \left[1, e^{-j2\pi\alpha}, \cdots, e^{-j2\pi(L-1)\alpha} \right]^{\mathsf{T}}$$

is a steering vector of length L. Symbol $\circ$ denotes the outer (tensor) product.

III. Parameter Estimation via Hankel Nuclear Norm Minimization (HNNM)

The process of parameter estimation utilizes the structure of the tensor $\boldsymbol{B}$. In this section, we first show that $\boldsymbol{B}$ can generate a low-rank 3-level Hankel matrix, then formulate a convex optimization to recover $\boldsymbol{B}$ from noisy measurements $\tilde{\boldsymbol{Y}}$, and finally extract delay-DoA-Doppler information.

A. Multilevel Hankel Matrix Construction

A Hankel matrix is a matrix of which each ascending skew-diagonal from left to right is constant. Let $\boldsymbol{b} \in \mathbb{C}^L$. A Hankel matrix $\boldsymbol{H} \in \mathbb{C}^{L_1 \times L_2}$, where $L_1 + L_2 = L + 1$, can be generated via

$$\boldsymbol{H} = \mathcal{H}(\boldsymbol{b}) = \begin{bmatrix} b_1 & b_2 & \cdots & b_{L_2} \\ b_2 & b_3 & \cdots & b_{L_2+1} \\ \vdots & \vdots & \ddots & \vdots \\ b_{L_1} & b_{L_1+1} & \cdots & b_L \end{bmatrix}.$$

The 3-way tensor $\boldsymbol{B}$ can generate a 3-level Hankel matrix. Let $L_1 + L_2 = L + 1$, $M_1 + M_2 = M + 1$, $N_1 + N_2 = N + 1$. A

3-level Hankel matrix $\boldsymbol{H} = \mathcal{H}^{\text{L3}}(\boldsymbol{B}) \in \mathbb{C}^{(L_1M_1N_1)\times(L_2M_2N_2)}$ can be generated recursively as follows [11]:

$$\boldsymbol{H}^{m,n} = \begin{bmatrix} B_{1,m,n} & B_{2,m,n} & \cdots & B_{L_2,m,n} \\ B_{2,m,n} & B_{3,m,n} & \cdots & B_{L_2+1,m,n} \\ \vdots & \vdots & \ddots & \vdots \\ B_{L_1,m,n} & B_{L_1+1,m,n} & \cdots & B_{L,m,n} \end{bmatrix},$$

$$\boldsymbol{H}^{n} = \begin{bmatrix} \boldsymbol{H}^{1,n} & \boldsymbol{H}^{2,n} & \cdots & \boldsymbol{H}^{M_2,n} \\ \boldsymbol{H}^{2,n} & \boldsymbol{H}^{3,n} & \cdots & \boldsymbol{H}^{M_2+1,n} \\ \vdots & \vdots & \ddots & \vdots \\ \boldsymbol{H}^{M_1,n} & \boldsymbol{H}^{M_1+1,n} & \cdots & \boldsymbol{H}^{M,n} \end{bmatrix},$$

$$\boldsymbol{H} = \begin{bmatrix} \boldsymbol{H}^{1} & \boldsymbol{H}^{2} & \cdots & \boldsymbol{H}^{N_2} \\ \boldsymbol{H}^{2} & \boldsymbol{H}^{3} & \cdots & \boldsymbol{H}^{N_2+1} \\ \vdots & \vdots & \ddots & \vdots \\ \boldsymbol{H}^{N_1} & \boldsymbol{H}^{N_1+1} & \cdots & \boldsymbol{H}^{N} \end{bmatrix},$$

where $\boldsymbol{H}^{m,n} \in \mathbb{C}^{L_1\times L_2}$ are 1-level Hankel matrices, $\boldsymbol{H}^{n} \in \mathbb{C}^{(L_1M_1)\times(L_2M_2)}$ are 2-level Hankel matrices. See Fig. 1 for an illustration.

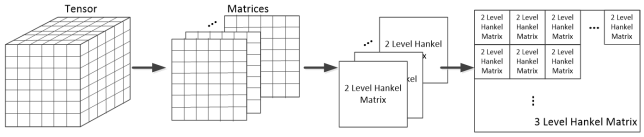

Fig. 1. An illustration of the 3-level Hankel matrix construction

A superposition of a small number of steering vectors generates a low-rank Hankel matrix. If $\boldsymbol{b} = \sum_{k=1}^{K} c_k \boldsymbol{a}^{L}(\alpha_k)$ where $c_k \neq 0$, then $\boldsymbol{H} = \mathcal{H}(\boldsymbol{b}) = \sum_{k=1}^{K} c_k \boldsymbol{a}^{L_1}(\alpha_k)\boldsymbol{a}^{L_2}(\alpha_k)^{\mathsf{T}}$. When $K < \min(L_1, L_2)$, $\boldsymbol{H}$ is rank-K Hankel matrix.

Similarly, a superposition of outer products of steering vectors can generate a low-rank multilevel Hankel matrix. For notational simplicity, rewrite tensor $\boldsymbol{B}$ in (7) as

$$\boldsymbol{B} = \sum_{k=1}^{K} c_k \boldsymbol{a}^{L}(\alpha_k) \circ \boldsymbol{a}^{M}(\beta_k) \circ \boldsymbol{a}^{N}(\gamma_k)$$

with nonzero c_k. It can be verified that

$$\boldsymbol{H} = \mathcal{H}^{\text{L3}}(\boldsymbol{B}) = \sum_{k=1}^{K} c_k \left(\boldsymbol{a}^{N_1}(\gamma_k) \otimes \boldsymbol{a}^{M_1}(\beta_k) \otimes \boldsymbol{a}^{L_1}(\alpha_k)\right) \left(\boldsymbol{a}^{N_2}(\gamma_k) \otimes \boldsymbol{a}^{M_2}(\beta_k) \otimes \boldsymbol{a}^{L_2}(\alpha_k)\right)^{\mathsf{T}},$$

where the symbol $\otimes$ denotes Kronecker product [18]. When K is sufficiently small, e.g., $K \ll \min(L_1M_1N_1, L_2M_2N_2)$, the 3-level Hankel matrix $\boldsymbol{H}$ is of low-K-rank.

B. The Convex Optimization Formulation of HNNM

By exploiting the low-K-rank structure of the 3-level Hankel matrix $\boldsymbol{H}$, we formulate a convex optimization problem for parameter estimation in the following Lasso form

$$\min_{\boldsymbol{B}} \ \frac{1}{2}\|\tilde{\boldsymbol{Y}} - \mathcal{A}(\boldsymbol{B})\|_F^2 + \lambda\|\mathcal{H}^{\text{L3}}(\boldsymbol{B})\|_*, \tag{8}$$

where $\|\cdot\|_F$ and $\|\cdot\|_*$ denote Frobenius and nuclear norms respectively, $\lambda > 0$ is a regularization constant appropriately chosen. As the objective function is not smooth, we apply alternating direction method of multipliers (ADMM) to solve it. The ADMM reformulation of (8) is given by

$$\begin{aligned} \min_{\boldsymbol{B},\boldsymbol{H}} \ & \frac{1}{2}\|\tilde{\boldsymbol{Y}} - \mathcal{A}(\boldsymbol{B})\|_F^2 + \lambda\|\boldsymbol{H}\|_*, \\ \text{s.t. } & \boldsymbol{H} = \mathcal{H}^{\text{L3}}(\boldsymbol{B}) \end{aligned} \tag{9}$$

The augmented Lagrangian for this problem is

$$\begin{aligned} L_\rho(\boldsymbol{B}, \boldsymbol{H}, \boldsymbol{v}) =& \frac{1}{2}\|\tilde{\boldsymbol{Y}} - \mathcal{A}(\boldsymbol{B})\|_F^2 + \lambda\|\boldsymbol{H}\|_* \\ & + \frac{\rho}{2}\|\boldsymbol{H} - \mathcal{H}^{\text{L3}}(\boldsymbol{B}) + \boldsymbol{v}/\rho\|_F^2 - \|\boldsymbol{v}\|_F^2/(2\rho), \end{aligned} \tag{10}$$

where ρ is a positive penalty parameter and $\boldsymbol{v}$ is the Lagrangian multiplier. (9) can be efficiently solved since ADMM admits closed form solutions: the update of $\boldsymbol{B}$ is a least squares problem; and the update of $\boldsymbol{H}$ can be solved by applying SVD and soft-thresholding function.

Let $\boldsymbol{B}^\star$ be the optimal solution obtained by solving (9). As long as $\boldsymbol{B}^\star$ is faithfully recovered, the delay, DoA, and Doppler can be jointly extracted from $\boldsymbol{B}^\star$ using the reduced-dimension MUSIC method developed in [22], which has the same performance as conventional MUSIC [12] but with significantly reduced computational complexity. In the near future, the ADMM process time could be further reduced by incorporating fast SVD methods.

IV. Numerical Implementation

In this section, we compare the joint delay-DoA-Doppler estimation performance of the proposed HNNM method with the on-grid algorithm OMP, and subspace method MUSIC.

TABLE I
OFDM signal specifications

Digital Modulation		4QAM
Carrier Frequency	f_c	300 MHz
Subcarrier Spacing	Δ_f	1 kHz
No. Subcarriers	N	36
OFDM Symbol Length	T	1 ms
Cyclic Prefix	T_{cp}	0.25 ms
OFDM Block Length	T'	1.25 ms
No. OFDM Blocks	M	5
No. Targets	K	3

The parameter settings of the OFDM signal applied in this simulation are shown in Table. I. The ground truth of delays, DoAs and Doppler shifts are illustrated in Table. II. We set the number of antenna elements $L = 7$. As for the OMP algorithm, we create a discrete grid with density of $[0 : 0.01 : 0.7] \times T_{cp}$ for τ_k, $[0^\circ : 1^\circ : 180^\circ]$ for θ_k and $[5 : 1 : 20]f_c/c$ for $f_{d,k}$. In generating the 3-level Hankel matrix in HNNM, we set $L_1 = 3$, $M_1 = 5$ and $N_1 = 4$.

Fig. 2 compares the performance of HNNM and MUSIC at SNR$=$ 10 dB, 0 dB and -5 dB. In all sub-figures, the grey vertical lines represent the values of the ground truth. It can be observed that HNNM performs well in estimating all

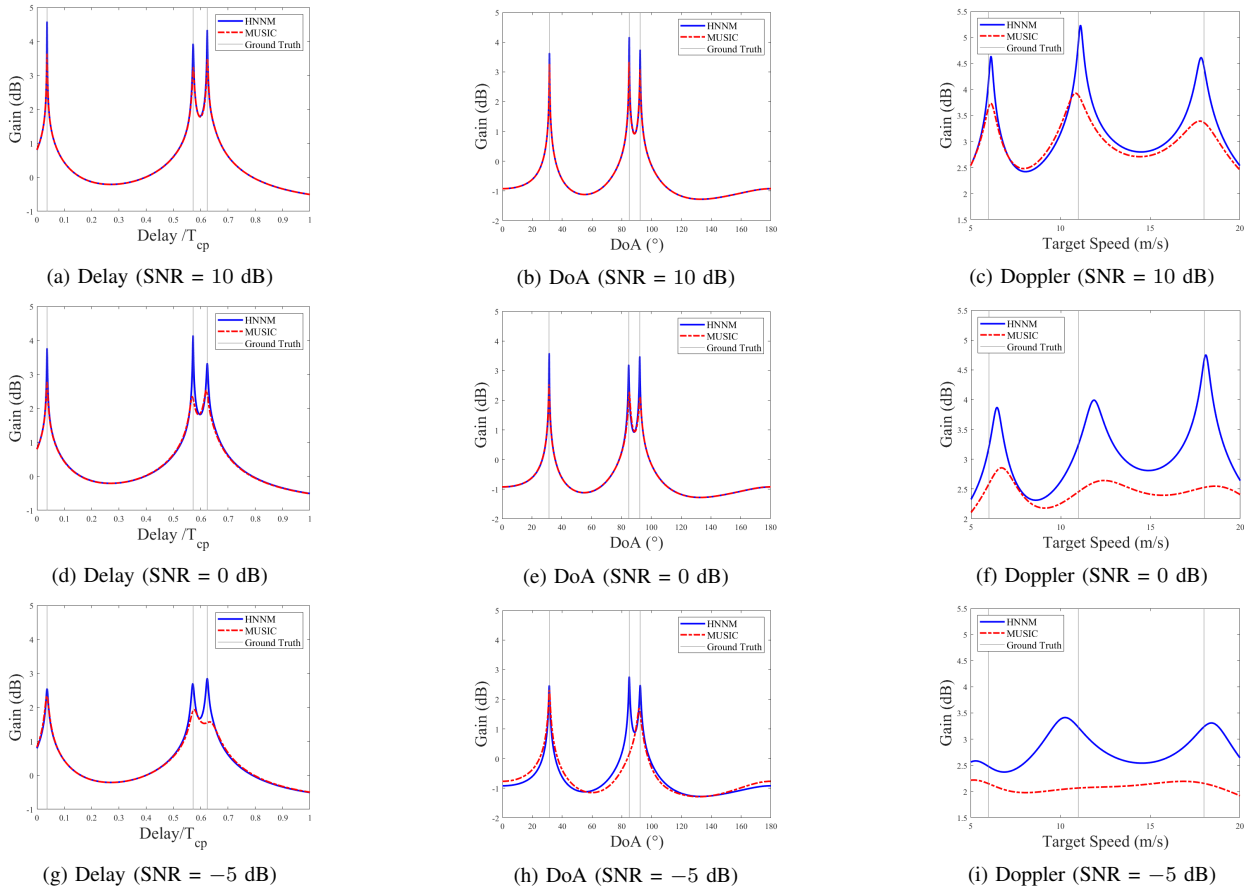

(a) Delay (SNR = 10 dB) (b) DoA (SNR = 10 dB) (c) Doppler (SNR = 10 dB)

(d) Delay (SNR = 0 dB) (e) DoA (SNR = 0 dB) (f) Doppler (SNR = 0 dB)

(g) Delay (SNR = -5 dB) (h) DoA (SNR = -5 dB) (i) Doppler (SNR = -5 dB)

Fig. 2. The delay, DoA and Doppler patterns at different SNRs. The red represents MUSIC, and the blue represents HNNM.

three parameters at SNR$=10$ dB, it gives accurate estimates of delay and DoA at SNR$=0$ dB and -5 dB, but its performance of Doppler estimation starts to deteriorate at SNR$=0$ dB and becomes only barely acceptable at SNR$=-5$ dB. By comparison, the performance of MUSIC in estimating delay and DoA is nearly as good as that of HNNM at SNR$=10$ dB and 0 dB, but becomes worse at SNR$=-5$ dB where MUSIC can only resolve two peaks rather than the ground truth three peaks. The performance of MUSIC for Doppler estimation is worse than HNNM under all the tested SNRs: when SNR$=-5$ dB, MUSIC fails to return meaningful estimations of Doppler. It can be concluded that HNNM performs better than MUSIC by exploiting the structure of $\boldsymbol{B}$.

Table. II compares the parameter estimation results of OMP with the ground truth at SNR$=10$ dB, 0 dB and -5 dB. An estimation is regarded successful if $\epsilon_{\text{delay}} < 0.02 \times T_{cp}$, $\epsilon_{\text{DoA}} < 2^\circ$ and $\epsilon_{Doppler} < f_c/c$, where ϵ represents the estimation error. Estimations marked in the blue color are those above the aforementioned bounds. Compare these to the estimation errors of HNNM at SNR$=-5$ dB given by $\epsilon_{\text{delay}} \approx 0.0003 \times T_{cp}$, $\epsilon_{\text{DoA}} \approx 0.1^\circ$, and $\epsilon_{\text{Doppler}} \approx 0.85 f_c/c$. Clearly HNNM performs much better than OMP. It is noteworthy that a further refinement of the discrete grid does not improve the performance of OMP at low SNR but results in larger computational complexity.

TABLE II
JOINT DELAY-DOA-DOPPLER ESTIMATION USING OMP

SNR	Delay τ ($\times T_{cp}$ s)	DoA θ ($^\circ$)	Doppler f_d ($\times f_c/c$)
Ground Truth	$[0.0371, 0.5724, 0.6243]$	$[31.5, 85.0, 92.3]$	$[6, 11, 18]$
10 dB	$[0.04, 0.55, 0.60]$	$[31, 88, 96]$	$[6, 14, 20]$
0 dB	$[0.04, 0.54, 0.60]$	$[31, 88, 96]$	$[6, 14, 20]$
-5 dB	$[0.05, 0.54, 0.60]$	$[31, 89, 96]$	$[5, 14, 20]$

We also measure the root mean squared error (RMSE) to evaluate the estimation accuracy of Delay, DoA and Doppler as RMSE $= \frac{1}{K}\sum_{k=1}^{K}\left(\frac{1}{N_t}\sum_{n_t}^{N_t}(p_k - \tilde{p}_{k,n_t})^2\right)^{\frac{1}{2}}$, where N_t, p and $\tilde{p}_{k,n_t}$ denote the number of Monte-Carlo trials, the ground truth of τ, θ and f_d for delay, DoA and Doppler estimation, and the estimates in the n_t-th trial, respectively. As shown in Fig. 3, the estimation error of these three methods tends to decrease as the SNR increases. While the proposed HNNM method has lower estimation error than that of MUSIC and OMP at all tested SNRs, the delay estimation error of HNNM is even below 3×10^{-3}, indicating that HNNM can recover all three parameters with good accuracy even at low SNRs.

It is also important to note that the ground truth parameters

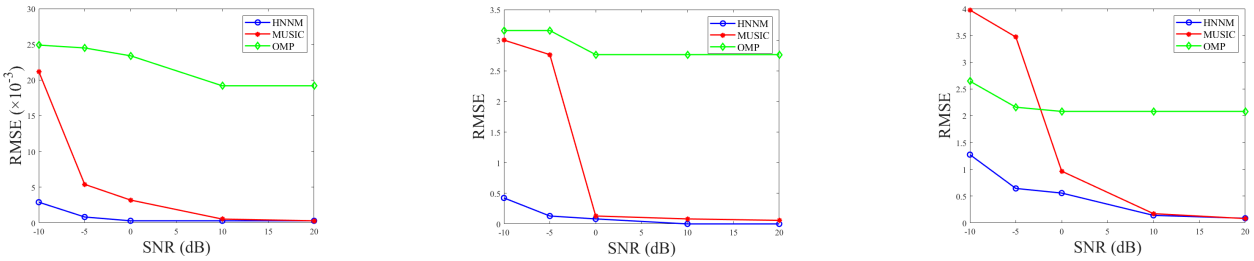

(a) Delay Estimation (b) DoA Estimation (c) Doppler Estimation

Fig. 3. Estimation accuracy for HNNM, MUSIC and OMP at different SNRs.

are chosen in such a way that the minimum gaps between them fall below the corresponding minimum separation bounds required by ANM. As shown in [10], [15], in ANM approach it is necessary to require the minimum gap in delay ($\Delta_f \tau$) as $\frac{2}{2N-1} = 0.028$, that in DoA ($\cos(\theta)$) as $\frac{2}{2L-1} = 0.15$, and that in Doppler ($f_d T'$) as $\frac{2}{2M-1} = 0.22$. In our simulations, the minimum gap in delay is $\Delta_f(0.6243 - 0.5724)T_{cp} = 0.013$, that in DoA is $|\cos(92.3°) - \cos(85°)| = 0.13$, that in Doppler is $2(11-6)T' = 0.0125$. All of them are below the corresponding minimum separation bounds.

V. Conclusions and Future Work

In this paper, a convex optimization is developed to jointly estimate delay, DoA and Doppler of back-scattered OFDM signals. It is based on a low-rank 3-level Hankel matrix that arises when the number of targets is small. Simulations demonstrate its robustness to noise and that it can go beyond the minimum separation required by ANM.

As future directions, it will be beneficial to incorporate fast SVD of Hankel matrix and speed-ups of ADMM into the optimization process so that larger system setup can be handled and faster convergence can be achieved.

References

[1] C. D. Ozkaptan, E. Ekici, O. Altintas, and C.-H. Wang, "OFDM pilot-based radar for joint vehicular communication and radar systems," in *2018 IEEE Vehicular Networking Conference (VNC)*. IEEE, 2018, pp. 1–8.

[2] Y. Liu, G. Liao, Y. Chen, J. Xu, and Y. Yin, "Super-resolution range and velocity estimations with OFDM integrated radar and communications waveform," *IEEE Transactions on Vehicular Technology*, vol. 69, no. 10, pp. 11 659–11 672, 2020.

[3] Y. Liu and Y. C. Eldar, "Joint radar-communications strategies for autonomous vehicles," *IEEE SIGNAL PROCESSING MAGAZINE*, vol. 1053, no. 5888/20, 2020.

[4] G. K. Carvajal, M. F. Keskin, C. Aydogdu, O. Eriksson, H. Herbertsson, H. Hellsten, E. Nilsson, M. Rydström, K. Vänas, and H. Wymeersch, "Comparison of automotive FMCW and OFDM radar under interference," in *2020 IEEE Radar Conference (RadarConf20)*. IEEE, 2020, pp. 1–6.

[5] C. R. Berger, B. Demissie, J. Heckenbach, P. Willett, and S. Zhou, "Signal processing for passive radar using OFDM waveforms," *IEEE Journal of Selected Topics in Signal Processing*, vol. 4, no. 1, pp. 226–238, 2010.

[6] S. F. Cotter, B. D. Rao, K. Engan, and K. Kreutz-Delgado, "Sparse solutions to linear inverse problems with multiple measurement vectors," *IEEE Transactions on Signal Processing*, vol. 53, no. 7, pp. 2477–2488, 2005.

[7] J. A. Tropp and A. C. Gilbert, "Signal recovery from random measurements via orthogonal matching pursuit," *IEEE Transactions on information theory*, vol. 53, no. 12, pp. 4655–4666, 2007.

[8] W. Dai and O. Milenkovic, "Subspace pursuit for compressive sensing signal reconstruction," *IEEE transactions on Information Theory*, vol. 55, no. 5, pp. 2230–2249, 2009.

[9] Y. Chi, L. L. Scharf, A. Pezeshki, and A. R. Calderbank, "Sensitivity to basis mismatch in compressed sensing," *IEEE Transactions on Signal Processing*, vol. 59, no. 5, pp. 2182–2195, 2011.

[10] G. Tang, B. N. Bhaskar, P. Shah, and B. Recht, "Compressed sensing off the grid," *IEEE transactions on information theory*, vol. 59, no. 11, pp. 7465–7490, 2013.

[11] Y. Chen and Y. Chi, "Robust spectral compressed sensing via structured matrix completion," *IEEE Transactions on Information Theory*, vol. 60, no. 10, pp. 6576–6601, 2014.

[12] R. Schmidt, "Multiple emitter location and signal parameter estimation," *IEEE transactions on antennas and propagation*, vol. 34, no. 3, pp. 276–280, 1986.

[13] Z. Yang and L. Xie, "Exact joint sparse frequency recovery via optimization methods," *IEEE Transactions on Signal Processing*, vol. 64, no. 19, pp. 5145–5157, 2016.

[14] J. He, H. Wymeersch, and M. Juntti, "Channel estimation for ris-aided mmwave mimo systems via atomic norm minimization," *IEEE Transactions on Wireless Communications*, vol. 20, no. 9, pp. 5786–5797, 2021.

[15] E. J. Candès and C. Fernandez-Granda, "Towards a mathematical theory of super-resolution," *Communications on pure and applied Mathematics*, vol. 67, no. 6, pp. 906–956, 2014.

[16] Y. Tsai, L. Zheng, and X. Wang, "Millimeter-wave beamformed full-dimensional mimo channel estimation based on atomic norm minimization," *IEEE Transactions on Communications*, vol. 66, no. 12, pp. 6150–6163, 2018.

[17] Y. Chi and M. F. Da Costa, "Harnessing sparsity over the continuum: Atomic norm minimization for superresolution," *IEEE Signal Processing Magazine*, vol. 37, no. 2, pp. 39–57, 2020.

[18] J. Ying, H. Lu, Q. Wei, J.-F. Cai, D. Guo, J. Wu, Z. Chen, and X. Qu, "Hankel matrix nuclear norm regularized tensor completion for n-dimensional exponential signals," *IEEE Transactions on Signal Processing*, vol. 65, no. 14, pp. 3702–3717, 2017.

[19] W. Xu, J. Yi, S. Dasgupta, J.-F. Cai, M. Jacob, and M. Cho, "Sep] ration-free super-resolution from compressed measurements is possible: an orthonormal atomic norm minimization approach," in *2018 IEEE International Symposium on Information Theory (ISIT)*. IEEE, 2018, pp. 76–80.

[20] S. Na, K. V. Mishra, Y. Liu, Y. C. Eldar, and X. Wang, "Tendsur: Tensor-based 4d sub-nyquist radar," *IEEE Signal Processing Letters*, vol. 26, no. 2, pp. 237–241, 2018.

[21] F. Athley, "Asymptotically decoupled angle-frequency estimation with sensor arrays," in *Conference Record of the Thirty-Third Asilomar Conference on Signals, Systems, and Computers (Cat. No. CH37020)*, vol. 2. IEEE, 1999, pp. 1098–1102.

[22] M. Feng, Z. Cui, Y. Yang, and Q. Shu, "A reduced-dimension MUSIC algorithm for monostatic FDA-MIMO radar," *IEEE Communications Letters*, vol. 25, no. 4, pp. 1279–1282, 2020.